frontiers | Frontiers in Materials

ORIGINAL RESEARCH
published: 28 June 2022
doi: 10.3389/fmats.2022.918091

Monitoring Damage Progression in Tensile Tested SiCp/Al Composites Using Acoustic Emission

Weiguo Wu[1], Wei Wei[1], Yanju Wang[2], Aixue Sha[2] and Wenfeng Hao[3]**

[1]Faculty of Civil Engineering and Mechanics, Jiangsu University, Zhenjiang, China, [2]Materials Evaluation Center for Aeronautical and Aeroengine Application, AECC Beijing Institute of Aeronautical Materials, Beijing, China, [3]College of Mechanical Engineering, Yangzhou University, Yangzhou, China

In this paper, the tensile tests of SiCp/Al composites were carried out, and the acoustic emission (AE) method was used to monitor the damage progress. The collected signals were analyzed in time-frequency domain. The AE signals were analyzed by principal component analysis (PCA) and fuzzy clustering method (FCM) to characterize the damage mode and failure mechanism of SiCp/Al composites. Three main damage modes of SiCp/Al composites were identified by FCM clustering: SiC/Al interface debonding, Al fracture and SiC particle fracture. After the tensile test, the fracture surface was analyzed by scanning electron microscope (SEM). The results of SEM and energy spectrum analysis confirmed the results of AE. The research results of this paper provide experimental support for the design and engineering application of SiCp/Al composites.

Keywords: SiCp/Al composites, failure mechanism, principal component analysis, acoustic emission, cluster analysis

OPEN ACCESS

Edited by:
Mauro Zarrelli,
National Research Council (CNR), Italy

Reviewed by:
Kemal Davut,
Izmir Institute of Technology, Turkey
Ehsan Ghassemali,
Jönköping University, Sweden
Angela Russo,
Università della Campania Luigi Vanvitelli, Italy

****Correspondence:***
Yanju Wang
yjwangbiam@163.com
Wenfeng Hao
hwf@yzu.edu.cn

Specialty section:
This article was submitted to Polymeric and Composite Materials, a section of the journal Frontiers in Materials

Received: *12 April 2022*
Accepted: *07 June 2022*
Published: *28 June 2022*

Citation:
Wu W, Wei W, Wang Y, Sha A and Hao W (2022) Monitoring Damage Progression in Tensile Tested SiCp/Al Composites Using Acoustic Emission. Front. Mater. 9:918091. doi: 10.3389/fmats.2022.918091

1 INTRODUCTION

SiCp/Al composites have high specific strength, high specific modulus, excellent thermal conductivity and wear resistance, low coefficient of thermal expansion and other excellent properties, which make them popular in military, automotive, microelectronic packaging, aerospace and other fields (Chen et al., 2009a; Xu et al., 2021; Cui et al., 2022; Dong et al., 2022; Lu et al., 2022). The study of the relationship between the macro mechanical properties and the micro structure of metal matrix composites can further reveal the internal strengthening mechanism of particle reinforced composites, which has important theoretical and practical significance for the design of particle reinforced composites and giving full play to the potential advantages of particle strengthening.

Many literatures have reported the testing and characterization of mechanical properties of SiCp/Al composites, and many important results and conclusions have been obtained (Christin, 2002; Chen et al., 2009b; Qian et al., 2015; Chen and Zhang, 2019; Sun et al., 2020; Di Caprio et al., 2021; Pereira et al., 2021). There are many studies on the friction properties of SiCp/Al composites. Lattanzi et al. (2022) studied the effect of Ni and Zr additions on hardness, elastic modulus and wear performance of Al-SiCp composite. Deng et al. (2020) conducted a comprehensive study on flank wear progression of polycrystalline diamond micro-tool during micro end-milling of SiCp/Al composites. (Zhu et al., 2019) studied the effects of particle size and surface modification of SiC on the wear behavior of high volume fraction Al/SiCp composites. Some scholars have studied the tensile and compressive properties of SiCp/Al composites. Yuan et al. (2021) studied the damage behavior and mechanism of SiCp/Al composites under biaxial tension. Shen et al. (2020) studied the

TABLE 1 | Chemical composition of 2009 Al alloy powder.

Components	Cu	Mg	Fe	Si	O	Al
wt%	3.2–4.4	1.0–1.6	<0.1	<0.1	<0.1	Bal.

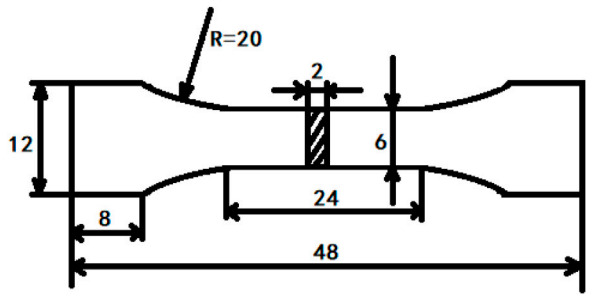

FIGURE 1 | Geometric dimension of the specimen (Unit: mm).

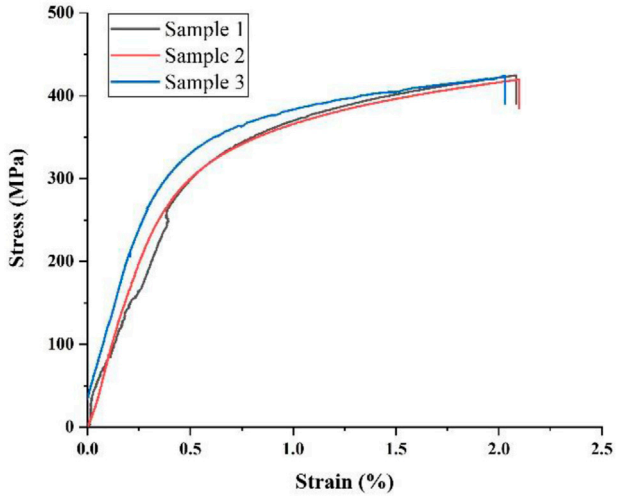

FIGURE 3 | Stress-strain curves of samples.

damage mechanism of 17vol% SiCp/Al composite under uniaxial tensile stress. Lee et al. (2018) studied the effects of SiC particulate size on dynamic compressive properties in 7075-T6 Al-SiCp composites. Zhang et al. (2018) conducted simulation on anisotropic load transfer and stress distribution in sicp/Al composites subjected to tensile loading. Other scholars have studied the fracture and damage mechanical behavior of SiCp/Al composites. Yu et al. (2021) conducted experimental and finite element method (FEM) study of cutting mechanism and damage behavior of ceramic particles in orthogonal cutting SiCp/Al composites. Pereira et al. (2021) conducted microstructural, mechanical, and facture characterization of metal matrix composite manufactured by accumulative roll bonding. Gao et al. (2019) studied strengthening and fracture behaviors in SiCp/Al composites with network particle distribution architecture. There are few reports on the judgment and identification of particle, matrix and interface failure modes in SiCp/Al composites, and the related experimental work is less involved.

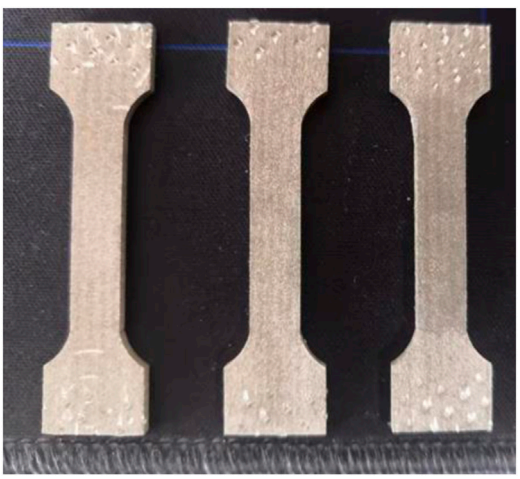

FIGURE 2 | Photos of samples.

Acoustic emission (AE) technology is widely used in mechanical property testing and failure analysis of materials because it can monitor the internal information in the process of material damage and fracture in real time (Loutas et al., 2017; Burud and Kishen, 2021; Wu and Kim, 2021). (Hao et al., 2019a; Zhao et al., 2019a; Zhao et al., 2019b; Hao et al., 2020) conducted experiments on failure of 3D braiding composite shafts using acoustic emission. (Hao et al., 2019b; Tang et al., 2020; Hao et al., 2021) conducted experiments on damage analysis of cylindrical lithium-ion cells under three-points bending using acoustic emission. (Thirukkumaran and Mukhopadhyay, 2021) characterized the damage mechanism during drilling of Al-5% SiC metal matrix composite using acoustic emission. AE counts, energy, peak amplitude, and root mean square voltage (AERMS) were correlated with cutting parameters (spindle speed and feed rate). The Fast Fourier Transform (FFT) and Continuous Wavelet Transform (CWT) of AE signals could identify the predominant peak frequency and time-frequency spectrum. The relationship between tool wear and AE parameter (wavelet coefficient) for different tool geometries was studied. Wavelet packet transform (WPT) was utilized to extract various AE source features present in the signals. (Mummery et al., 1993) used acoustic emission in tensile testing of particulate-reinforced metal matrix composites, they used the size and number of emissions as a function of strain. This has been shown to be simply related to the rate of void nucleation at the reinforcing phase. Both particle fracture and particle/matrix decohesion mechanisms can be detected. Void nucleation was observed from the onset of plastic deformation and a linear relationship between damage initiation rate and strain was found. The rate of emission increased with reinforcing particle size and volume fraction but was independent of matrix alloy composition and heat treatment. These results show that the failure strain of

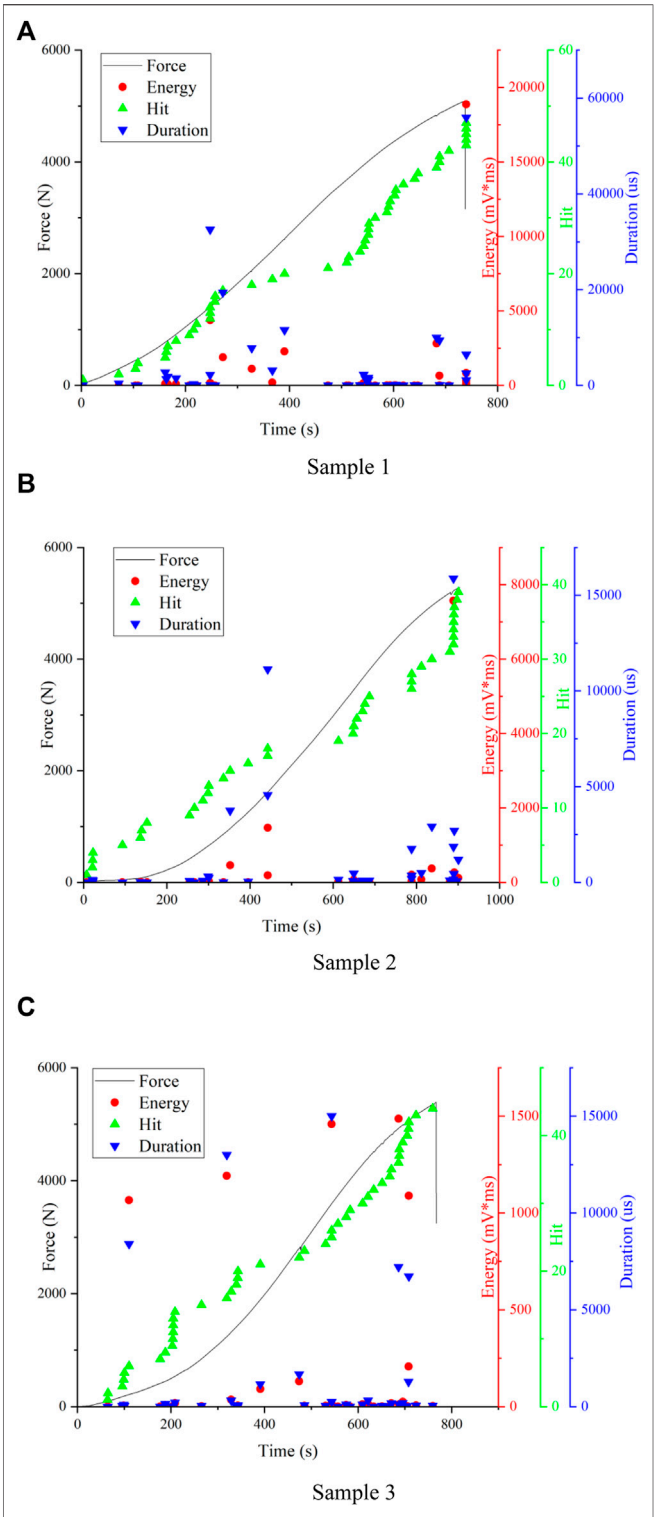

FIGURE 4 | Force/energy/hits/duration time. **(A)** sample 1; **(B)** sample 2; **(C)** sample 3.

particulate metal matrix composites is not controlled solely by the onset of void nucleation at the reinforcing phase. Local failure processes in the matrix are shown to promote void coalescence and dominate the ductility. (Neu and Roman, 1994) used AE to monitor damage in metal-matrix composites subjected to thermomechanical fatigue. Pacheco et al. (1998) studied the effects of matrix and fiber properties on the mechanical behavior and AE in continuous fiber reinforced metal matrix composites.

AE technology has been widely used in particle reinforced metal matrix composites. However, the quantitative relationship between particle fracture, matrix fracture, interfacial debonding and AE parameters in particle reinforced metal matrix composites is still an open question. In this paper, the tensile tests of SiCp/Al composites were carried out, and the AE method was used to monitor the damage progress. The collected signals were analyzed in time-frequency domain. The AE signals were analyzed by principal component analysis (PCA) and fuzzy clustering method (FCM) to characterize the damage mode and failure mechanism of SiCp/Al composites. Three main damage modes of SiCp/Al composites were identified by FCM clustering: SiC/Al interface debonding, Al fracture and SiC particle fracture. After the tensile test, the fracture surface was analyzed by scanning electron microscope (SEM). The results of SEM and energy spectrum analysis confirmed the results of acoustic emission.

2 EXPERIMENTAL DETAILS

2.1 Samples

The material used in this paper is 15% SiCp/2009Al composite. The matrix of the composite is 2009 Al, and its alloy composition is listed in **Table 1**. Selection of reinforcing particles α- SiC, where the particle size is 8 μ m and the volume fraction is 15%. The preparation process of composite materials adopts powder metallurgy method, and its process flow is as follows: firstly, 2009 aluminum alloy powder is prepared by supersonic gas atomization method. Then, SiC powder and 2009Al powder are finely mixed, and the mixed composite powder is put into the package. After vacuum degassing, hot isostatic pressing is carried out. Then the hot isostatic pressing ingot is hot extruded on a extruder with an extrusion ratio of 9:1.

The geometric diagram of the sample is shown in **Figure 1**. The gauge length is 24 mm, the width is 6 mm and the thickness is 2 mm. The sample prepared after processing is shown in **Figure 2**.

2.2 Experimental Setups

In this paper, the tensile properties of SiCp/Al composites were tested by universal testing machine, and the loading rate was 0.5 mm/min. Attach a strain gauge to the sample and use the uT7110Y static strain instrument to obtain the strain data during loading. The sampling frequency is 2 Hz. At the same time, the acoustic emission signal is collected and analyzed by DS5-32B full information acoustic emission signal analyzer. The acquisition accuracy is 16 bit, the sampling rate is 3 MHz, and the sampling time interval is 0.3333 μ s. The threshold trigger mode is adopted, and the channel threshold value is 100 mV. The diameter of the acoustic emission sensor is

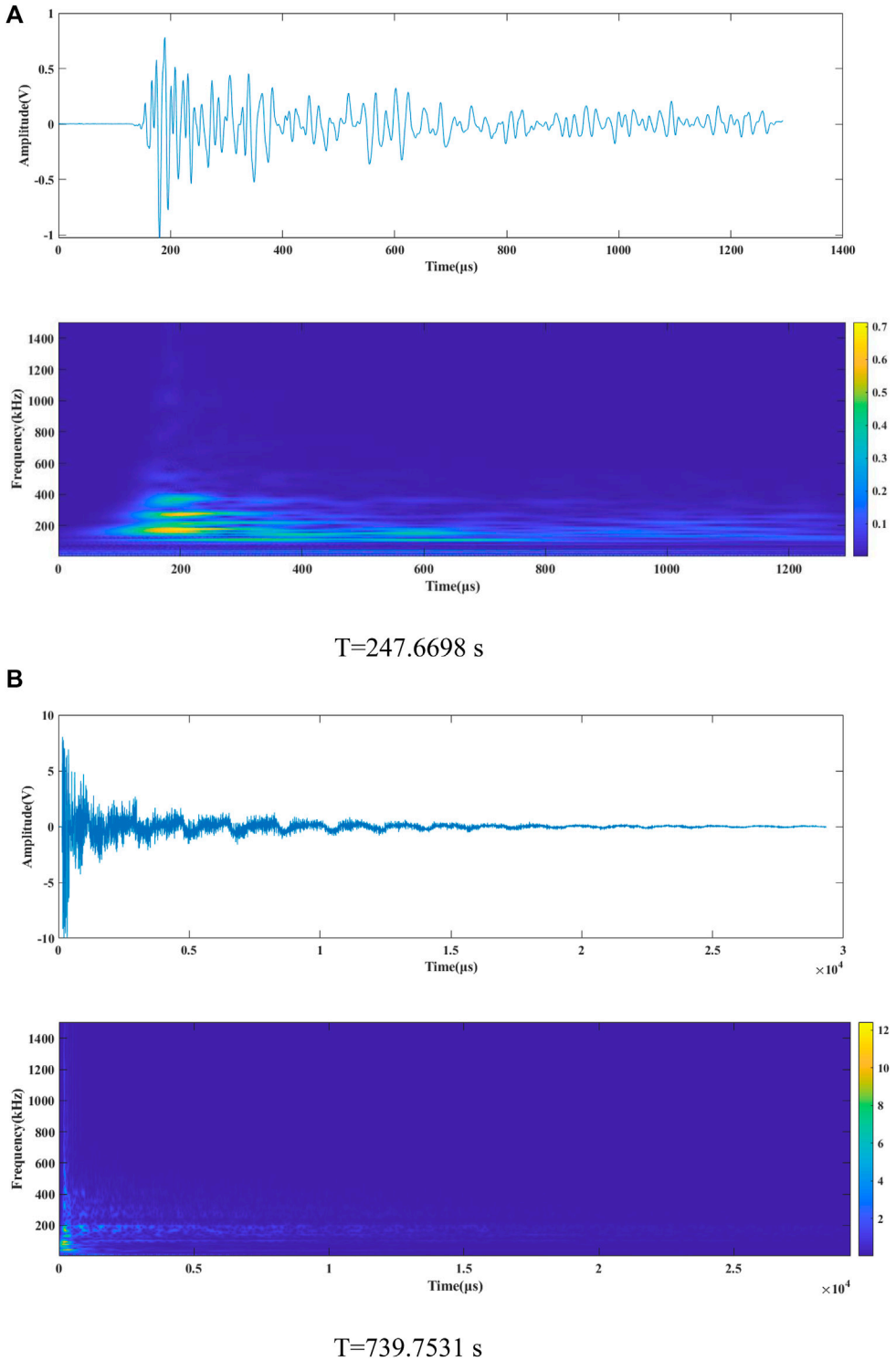

FIGURE 5 | Waveform and continuous wavelet transform diagram. **(A)** T = 247.6698 s; **(B)** T = 739.7531 s.

19 mm. Before the experiment, fix the sensor in the middle of the sample with insulating tape to reduce the waveform loss. Silicone grease coupling agent is coated between the sensor and the sample to reduce the omission of acoustic emission signal information. The sensor is connected to the equipment with 60 dB smart AE preamplifier. The data of each experimental device is transmitted to the data acquisition system on the corresponding computer.

TABLE 2 | Pearson correlation coefficient of characteristic parameters of AE signal of sample 1.

	Amplitude	Duration	Rise Time	Ringing Count	Rise Count	Energy	Centroid Frequency	Peak Frequency
Amplitude	1.000	0.636	0.252	0.791	0.299	0.673	0.402	0.440
Duration	0.636	1.000	0.342	0.836	0.080	0.931	0.141	0.021
Rise time	0.252	0.342	1.000	0.132	0.530	0.198	-0.033	-0.097
Ringing count	0.791	0.836	0.132	1.000	0.107	0.942	0.307	0.247
Rise count	0.299	0.080	0.530	0.107	1.000	0.030	0.217	0.316
Energy	0.673	0.931	0.198	0.942	0.030	1.000	0.222	0.130
Centroid frequency	0.402	0.141	-0.033	0.307	0.217	0.222	1.000	0.799
Peak frequency	0.440	0.021	-0.097	0.247	0.316	0.130	0.799	1.000

TABLE 3 | Common factor variance of characteristic parameter (sample 1).

	Amplitude	Duration	Rise Time	Ringing Count	Rise Count	Energy	Centroid Frequency	Peak Frequency
Initial value	1	1	1	1	1	1	1	1
Extract value	0.775	0.916	0.841	0.941	0.832	0.957	0.834	0.916

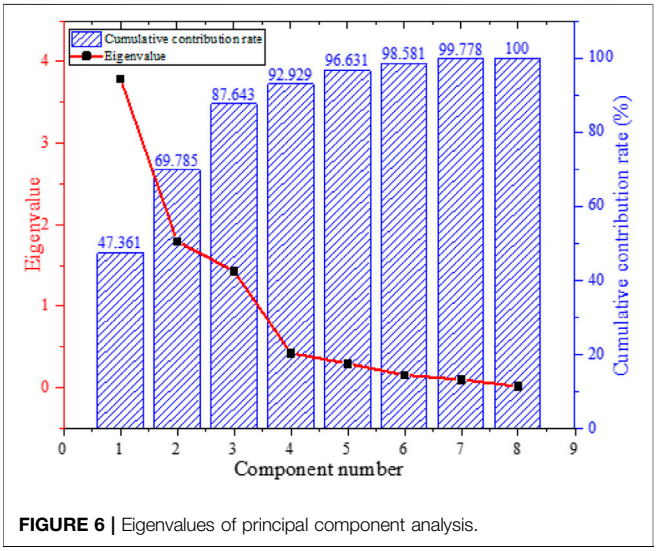

FIGURE 6 | Eigenvalues of principal component analysis.

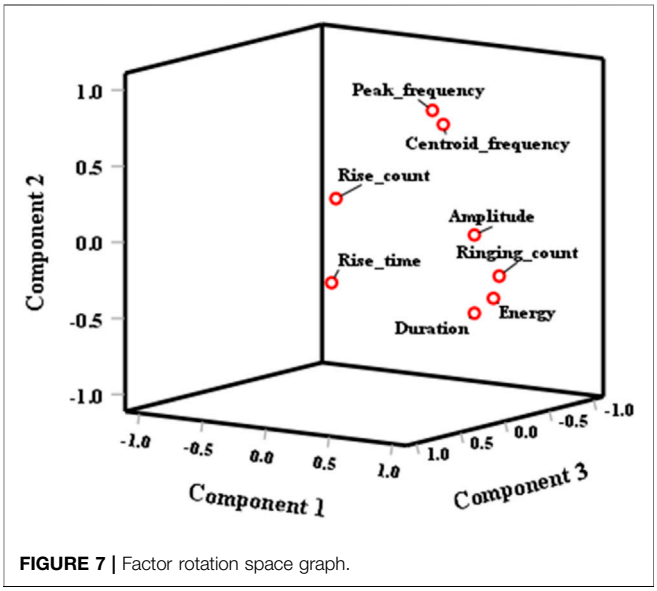

FIGURE 7 | Factor rotation space graph.

3 RESULTS AND DISCUSSION

The load data obtained by the universal testing machine is converted into engineering stress data through calculation, the strain data obtained by the strain gauge is processed, and the stress-strain curve of each sample is drawn, as shown in **Figure 3**. The average yield strength of the studied materials is 258 MPa, the average tensile strength is 438 MPa, and the average elongation is 4.167%.

AE signal characteristic parameter analysis is a common method to study damage signals. This method extracts the characteristic parameters of time domain or frequency domain waveform, such as impact number, amplitude, energy, rise time, duration, ring count, peak frequency, etc., characterizes the characteristics of acoustic emission source according to the change trend of characteristic parameters, and then explains the damage state of samples. The significance of common AE signal characteristic parameters is introduced below:

1) Hit: any signal that exceeds the threshold and causes the channel to obtain data is called an impact, which reflects the total amount and frequency of AE activity and is commonly used for AE activity evaluation.
2) Amplitude: the maximum amplitude value of the signal waveform, which is related to the size of AE events and is not affected by the threshold. It directly determines the

TABLE 4 | Correlation coefficient between principal components and characteristic parameters (sample 1).

	Components		
	1	2	3
Amplitude	0.876	0.090	0.008
Duration	0.854	−0.431	−0.023
Rise time	0.330	−0.158	0.841
Ringing count	0.927	−0.205	−0.199
Rise count	0.313	0.382	0.767
Energy	0.896	−0.351	−0.179
Centroid frequency	0.487	0.747	−0.196
Peak frequency	0.432	0.840	−0.152

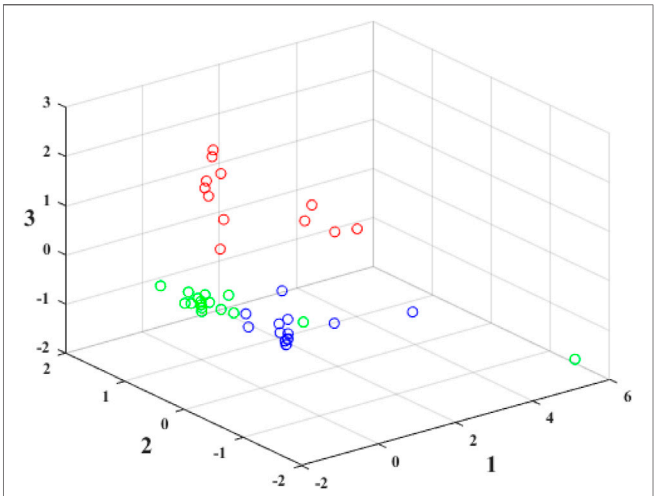

FIGURE 8 | FCM clustering diagram of PCA results.

TABLE 5 | 20–80% principal component range table (sample 1).

	Component 1	Component 2	Component 3
Cluster 1	−0.810, −0.470	−0.964, −0.730	−0.394, −0.145
Cluster 2	−0.273, 0.147	0.489, 1.103	−0.982, −0.681
Cluster 3	0.110, 0.634	−1.185, 1.164	1.021, 1.855

testability of AE events. It is commonly used for wave source type identification and intensity measurement.

3) Duration: the time interval between the first time the AE signal crosses the threshold and the last time the AE signal exceeds the threshold in a complete AE event. Similar to ring counting, it is often used for special wave source types and noise identification, and can reflect the strength and frequency of the signal.
4) Rise time: the time interval that the signal reaches the maximum amplitude after crossing the threshold for the first time. Due to the influence of propagation, its physical meaning is not clear, but it is often used for electromechanical noise identification in AE signal analysis.

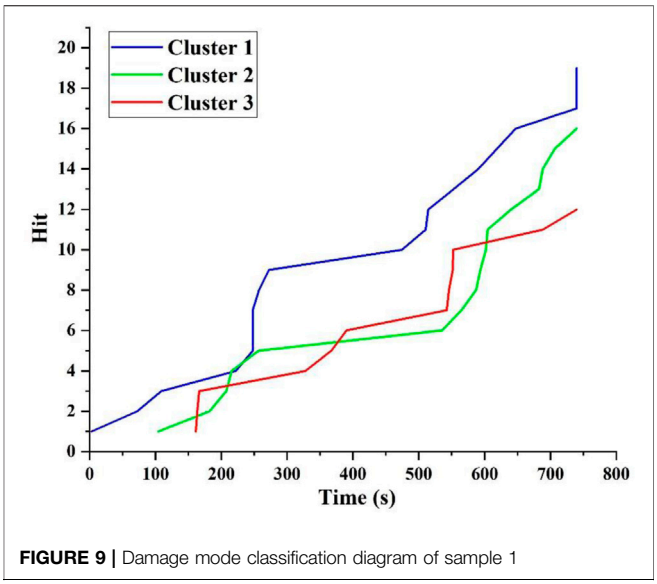

FIGURE 9 | Damage mode classification diagram of sample 1

5) Ringing count: ringing pulse counting across threshold, which is often used to evaluate the activity of AE signal.
6) Energy: the area under the envelope of AE signal, which reflects the relative energy and intensity of the event and is insensitive to the threshold, propagation characteristics and working frequency.
7) Centroid frequency: the frequency of the energy center of gravity of AE signal after Fourier transform. This frequency is usually used to study the range of damaged frequency band.
8) Peak frequency: the frequency corresponding to the peak point in the frequency domain of AE signal. The distribution of peak frequency can roughly reflect the occurrence of different types of damage.

The hits, energy and duration extracted from the characteristic parameters of AE signal are shown in **Figure 4**. The time domain analysis of AE signal shows that the experimental process is divided into two stages. In the early stage of the first stage, the hits of AE signal increases slowly, the energy is very low and the duration is very short. In the middle of the first stage, the number of hits increases rapidly, the energy increases suddenly, and the duration increases suddenly, which may indicate the beginning of internal damage of the sample. In the later stage of the first stage, the hits increase slows down, the energy decreases and the duration decreases. In the second stage, the number of hits increases rapidly, indicating that a large amount of damage may be occurring in the sample at this time. In the later stage of the second stage, the energy increases suddenly and reaches the peak, and the duration increases suddenly and reaches the peak, which corresponds to the final fracture of the sample.

AE signals from the first group of experiments are extracted for continuous wavelet transform analysis, as shown in **Figure 5**. In this paper, the complex Morlet wavelet transform cmor3-3 is selected for analysis because it has a good balance between time and frequency localization, and it provides smooth and continuous amplitude. Energy, duration and time-frequency

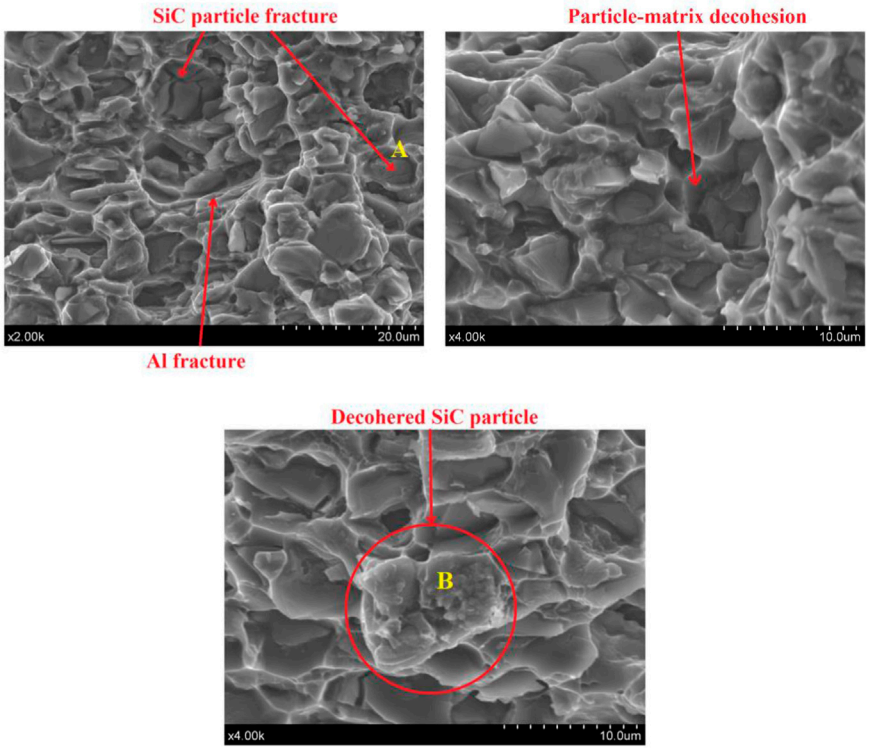

FIGURE 10 | SEM secondary electron micrographs of fracture surface of specimens.

analysis show that when t = 247.6698 s, the frequency of AE signal is not higher than 400 kHz, the energy is 4,387.94 mV * ms, and the duration is 32,560.33 μ s. This corresponds to the AE signal sent when the damage in the sample begins. When t = 739.7531 s, the frequency of AE signal fluctuates between 20 and 600 kHz, the energy reaches 18,872.57 mV * ms, and the duration reaches 55,945.33 μ s. This corresponds to the continuous AE signal emitted when the sample breaks.

The amplitude, duration, rise time, ring count, energy, hits, centroid frequency and peak frequency of AE signals in the first group of experiments were selected for principal component analysis. On the basis of maintaining the integrity of information, a simple visual analysis is provided to describe the characteristics of AE signals.

Table 2 shows the Pearson correlation coefficients of the characteristic parameters of the AE signal of sample 1. It can be seen from **Table 2** that some characteristic parameters have very good correlation (ex: Energy vs. Duration, Energy vs. Ringing count, Amplitude vs. Ringing Count). On the other hand, the correlation coefficient is almost ZERO for some other parameters (Rise Count vs. Duration, Rise time vs. Centroid frequency, Energy vs. Rise count). Kmo test result is 0.601 and Bartlett sphericity test result is 0.000. Therefore, the above characteristic parameters are applicable to principal component analysis.

The characteristic parameters of 8 AE signals were analyzed by principal component analysis. **Table 3** shows the common factor variance of principal component analysis of 8 characteristic parameters of sample 1. It can be seen from **Table 3** that these eight variables have high commonality, and most of the information in the variables can be extracted by factors, so the PCA results are effective.

Figure 6 shows that the characteristic value of the first three components is greater than 1, and the cumulative contribution rate of the first three components is 87.643%, which represents the overall characteristics of AE signal. Therefore, sample 1 can only select the first three components as the main components of PCA.

The purpose of principal component analysis is not only to extract common factors and reduce dimension, but also to get the practical significance of each common factor, so as to make a scientific analysis of practical problems. In order to make the coefficients in the factor load matrix more significant, the initial factor load matrix is rotated. The rotation does not change the overall result of principal component analysis, but affects the load distribution of each factor on each variable and the contribution rate of each factor. After rotation, it is easier to get the actual meaning of each common factor. The extracted three components are analyzed, and the spatial diagram of factor rotation is shown in **Figure 7**. The composition correlation table of 8 AE characteristic parameters is shown in **Table 4**.

It can be seen that the amplitude and duration of AE signal 1 and 4 are mainly positively correlated with AE signal in time domain; The peak frequency and centroid frequency of AE signal have a great influence on principal component 2; The rise time and rise count of AE signal have the greatest impact on principal component 3, reflecting the waveform shape characteristics.

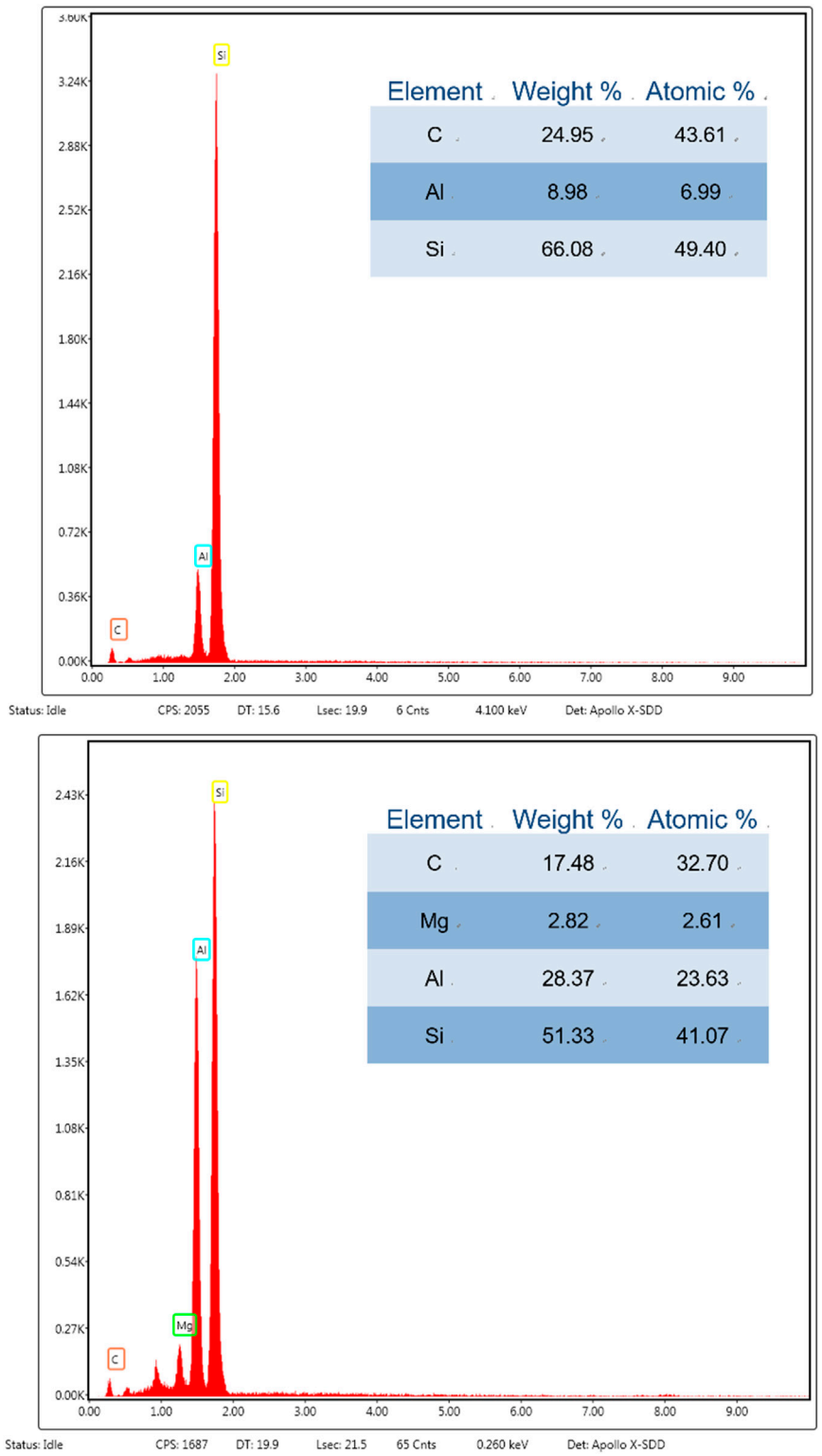

FIGURE 11 | EDS analysis results of regions identified in **Figure 11**.

The internal damage of Al/SiC particles during FCM loading is analyzed by clustering, and the internal damage of SiC particles is obtained. The results of FCM analysis are shown in **Figure 8**. Considering the factor of data dispersion, in order to characterize the overall level of clustering, take the score of 20–80% principal component value of clustering for statistics. The greater the

absolute value of the principal component value of a cluster, the greater the influence of this principal component on clustering. The statistical results are shown in **Table 5**.

Cluster 1: the absolute value of principal component 1 is large and negative, that is, it is a strong negative correlation; The absolute value of principal component 2 is large, which has a strong negative correlation; The absolute value of principal component 3 is small, which is a weak negative correlation.

Cluster 2: the value of principal component 1 is −0.273–0.147, that is, the difference of each characteristic parameter is small, which is at the average level; The value of principal component 2 is large and positive, which is a strong positive correlation; The absolute value of principal component 3 is large and has a strong negative correlation.

Cluster 3: the value of principal component 1 is large and positive, that is, it is a strong positive correlation. The distribution of principal component 2 is discrete at the medium level; The value of principal component 3 has a strong positive correlation.

The distribution of the three clusters on the time axis is shown in **Figure 9**. It can be seen from **Figure 9** that cluster 1 runs through the whole loading process, and the number of AE hits is the largest in the whole loading process. Therefore, cluster 1 is Al-matrix fracture, and the main characteristics of AE signal are low frequency, short duration, low energy, amplitude and ringing count. Cluster 2 starts to appear later than cluster 1, and its AE hits are lower than cluster 1. Therefore, cluster 2 is SiC/Al interface decohesion, which is characterized by short rise time, low rise count and high frequency. Cluster 3 starts to appear later than the other two classifications. Therefore, cluster 3 is SiC fracture, with high AE signal energy, amplitude and ring count, long duration, long rise time, high rise count and discrete frequency distribution.

The SEM secondary electron micrographs of fracture surface of specimens are shown in **Figure 10**. Three damage modes were observed in these SEM images: SiC/Al interface decohesion, Al fracture and SiC particle fracture. The energy dispersive X-ray spectroscopy (EDS) analysis results of regions identified in **Figure 10** (**Figure 11**) show that the main surface elements are silicon, aluminum, carbon and magnesium. The content of silicon is higher than that of aluminum, which proves that the main component of the selected area is silicon carbide.

4 CONCLUSION

In this paper, the tensile tests of SiCp/Al composites were carried out on the universal testing machine, and the AE method was used to monitor the damage progress. The collected signals were analyzed in time-frequency domain. At the same time, the AE signals were analyzed by PCA and FCM to characterize the damage mode and mechanism of SiCp/Al composites. Three main damage modes of SiCp/Al composites were identified by FCM clustering: SiC/Al interface debonding, Al fracture and SiC particle fracture. After the tensile test, the fracture surface was analyzed by SEM. The results of SEM image and energy spectrum analysis confirmed the results of acoustic emission analysis. The results show that cluster 1 runs through the whole loading process, and the number of AE hits is the largest in the whole loading process. Therefore, cluster 1 is Al-matrix fracture, and the main characteristics of AE signal are low frequency, short duration, low energy, amplitude and ringing count. Cluster 2 starts to appear later than cluster 1, and its AE hits are lower than cluster 1. Therefore, cluster 2 is SiC/Al interface decohesion, which is characterized by short rise time, low rise count and high frequency. Cluster 3 starts to appear later than the other two classifications. Therefore, cluster 3 is SiC fracture, with high AE signal energy, amplitude and ring count, long duration, long rise time, high rise count and discrete frequency distribution (Mummery et al., 1993).

DATA AVAILABILITY STATEMENT

The original contributions presented in the study are included in the article/Supplementary Material, further inquiries can be directed to the corresponding authors.

AUTHOR CONTRIBUTIONS

Author Contributions: WWu: Investigation, Data curation, Writing- Original draft preparation. WWe: Software, Validation. YW: Conceptualization, Methodology, Supervision. AS: Software, Conceptualization, Methodology, Supervision. WH: Conceptualization, Methodology, Writing- Reviewing and Editing.

FUNDING

The authors are grateful for the financial support provided by the Six Talent Peaks Project in Jiangsu Province (Grant Nos. 2019-KTHY-059).

REFERENCES

Burud, N. B., and Kishen, J. M. C. (2021). Response Based Damage Assessment Using Acoustic Emission Energy for Plain Concrete. *Constr. Build. Mater.* 269, 121241. doi:10.1016/j.conbuildmat.2020.121241

Chen, B., and Zhang, G. (2019). Dissimilar Joining of Pure Aluminum to SiCp/Al-MMCs Using an AlMgGaLi Active Interlayer Foil. *J. Materi Eng Perform* 28, 5289–5298. doi:10.1007/s11665-019-04270-1

Chen, X. W., Zhang, T. J., and Liu, S. H. (2009). Accelerated Ageing Behavior of PMMA under Hygrothermal Air and Water Conditions. *Fail. Analysis Prev.* 4, 193–195.

Chen, X. W., Pei, G. L., and Jin, Y. S. (2009). Study on Accelerated Ageing of Aeronautical Perspex(PMMA) in Ultraviolet. *J. Aeronautical Mater.* 29, 107–112.

Christin, F. (2002). Design, Fabrication, and Application of Thermostructural Composites (TSC) like C/C, C/SiC, and SiC/SiC Composites. *Adv. Eng. Mat.* 4, 903–912. doi:10.1002/adem.200290001

Cui, Q., Ma, L., Zhu, C., Zhou, C., Song, Y., and Liang, J. (2022). Grain Refinement and Mechanical Property Improvements in Ultrasound-Assisted Brazing of SiCp/Al Composite Materials. *J. Mater Eng. Perform.* 31, 4974–4982. doi:10.1007/s11665-022-06578-x

Deng, B., Peng, F., Zhou, L., Wang, H., Yang, M., and Yan, R. (2020). A Comprehensive Study on Flank Wear Progression of Polycrystalline Diamond Micro-tool during Micro End-Milling of SiCp/Al Composites. *Wear* 456-457, 203291. doi:10.1016/j.wear.2020.203291

Di Caprio, F., Russo, A., Manservigi, C., Scigliano, R., De Stefano Fumo, M., Tescione, D., et al. (2021). Damage Tolerance Evaluation of a C/C-SiC Composite Body Flap of a Re-entry Vehicle. *Compos. Struct.* 274, 114341. doi:10.1016/j.compstruct.2021.114341

Dong, C., Wang, R., Wang, X., and Zhou, L. Hot Deformation Characteristics and Microstructure Evolution of SiCp/Al2014 Composite Fabricated by Powder Metallurgy. *J. Mater Eng. Perform.* 31 (2022), 221–229. doi:10.1007/s11665-021-06151-y

Gao, X., Zhang, X., and Geng, L. (2019). Strengthening and Fracture Behaviors in SiCp/Al Composites with Network Particle Distribution Architecture. *Mater. Sci. Eng. A* 740-741, 353–362. doi:10.1016/j.msea.2018.10.105

Hao, W., Yuan, Z., Tang, C., Zhang, L., Zhao, G., and Luo, Y. (2019). Acoustic Emission Monitoring of Damage Progression in 3D Braiding Composite Shafts during Torsional Tests. *Compos. Struct.* 208, 141–149. doi:10.1016/j.compstruct.2018.10.011

Hao, W., Yuan, Z., Xu, Y., Zhu, S., Chen, H., and Fang, D. (2019). Damage Analysis of Cylindrical Lithium-Ion Cells under Three-Points Bending Using Acoustic Emission. *J. Power Sources* 444, 227323. doi:10.1016/j.jpowsour.2019.227323

Hao, W., Huang, Z., Xu, Y., Zhao, G., Chen, H., and Fang, D. (2020). Acoustic Emission Characterization of Tensile Damage in 3D Braiding Composite Shafts. *Polym. Test.* 81, 106176. doi:10.1016/j.polymertesting.2019.106176

Hao, W., Yuan, Z., Li, D., Zhu, Z., and Jiang, S. (2021). Study on Mechanical Properties and Failure Mechanism of 18650 Lithium-Ion Battery Using Digital Image Correlation and Acoustic Emission. *J. Energy Storage* 41, 102894. doi:10.1016/j.est.2021.102894

Lattanzi, L., Etienne, A., Li, Z., Chandrashekar, G. T., Gonapati, S. R., Awe, S. A., et al. (2022). The Effect of Ni and Zr Additions on Hardness, Elastic Modulus and Wear Performance of Al-SiCp Composite. *Tribol. Int.* 169, 107478. doi:10.1016/j.triboint.2022.107478

Lee, H., Choi, J. H., Jo, M. C., Lee, D., Shin, S., Jo, I., et al. (2018). Effects of SiC Particulate Size on Dynamic Compressive Properties in 7075-T6 Al-SiCp Composites. *Mater. Sci. Eng. A* 738, 412–419. doi:10.1016/j.msea.2018.09.082

Loutas, T., Eleftheroglou, N., and Zarouchas, D. (2017). A Data-Driven Probabilistic Framework towards the *In-Situ* Prognostics of Fatigue Life of Composites Based on Acoustic Emission Data. *Compos. Struct.* 161, 522–529. doi:10.1016/j.compstruct.2016.10.109

Lu, S., Wang, X., Teng, L., Zhang, J., Zhou, Z., Tong, Z., et al. Finite Element Analysis and Experimental Investigation of Ultrasonic Testing of Internal Defects in SiCp/Al Composites. *Ceram. Int.* 48 (2022), 5972–5982. doi:10.1016/j.ceramint.2021.11.133

Mummery, P. M., Derby, B., and Scruby, C. B. (1993). Acoustic Emission from Particulate-Reinforced Metal Matrix Composites. *Acta Metallurgica Materialia* 41, 1431–1445. doi:10.1016/0956-7151(93)90252-n

Neu, R. W., and Roman, I. (1994). Acoustic Emission Monitoring of Damage in Metal-Matrix Composites Subjected to Thermomechanical Fatigue. *Compos. Sci. Technol.* 52, 1–8. doi:10.1016/0266-3538(94)90002-7

Pacheco, T., Nayeb-Hashemi, H., and Sallam, H. E. M. (1998). The Effects of Matrix and Fiber Properties on the Mechanical Behavior and Acoustic Emission in Continuous Fiber Reinforced Metal Matrix Composites. *Mater. Sci. Eng. A* 247, 88–96. doi:10.1016/s0921-5093(97)00766-1

Pereira, G. S., Da Silva, E. P., Requena, G. C., Avila, J. A., and Tarpani, J. R. Microstructural, Mechanical, and Fracture Characterization of Metal Matrix Composite Manufactured by Accumulative Roll Bonding. *J. Mater Eng. Perform.* 30 (2021), 2645–2660. doi:10.1007/s11665-021-05619-1

Qian, C.-h., Li, P., and Xue, K.-m. (2015). Thermal Properties of SiCp/Al Composites Consolidated by Equal Channel Angular Pressing and Torsion. *J. Materi Eng Perform* 24, 832–838. doi:10.1007/s11665-014-1319-7

Shen, Q., Yuan, Z., Liu, H., Zhang, X., Fu, Q., and Wang, Q. (2020). The Damage Mechanism of 17vol.%SiCp/Al Composite under Uniaxial Tensile Stress. *Mater. Sci. Eng. A* 782, 139274. doi:10.1016/j.msea.2020.139274

Sun, W., Duan, C., and Yin, W. (2020). Development of a Dynamic Constitutive Model with Particle Damage and Thermal Softening for Al/SiCp Composites. *Compos. Struct.* 236, 111856. doi:10.1016/j.compstruct.2020.111856

Tang, C., Yuan, Z., Liu, G., Jiang, S., and Hao, W. (2020). Acoustic Emission Analysis of 18,650 Lithium-Ion Battery under Bending Based on Factor Analysis and the Fuzzy Clustering Method. *Eng. Fail. Anal.* 117, 104800. doi:10.1016/j.engfailanal.2020.104800

Thirukkumaran, K., and Mukhopadhyay, C. K. Analysis of Acoustic Emission Signal to Characterization the Damage Mechanism during Drilling of Al-5%SiC Metal Matrix Composite. *Silicon-Neth.* 13 (2021), 309–325. doi:10.1007/s12633-020-00426-0

Wu, K., and Kim, J. (2021). Acoustic Emission Monitoring during Open-Morphological Pitting Corrosion of 304 Stainless Steel Passivated in Dilute Nitric Acid. *Corros. Sci.* 180, 109224. doi:10.1016/j.corsci.2020.109224

Xu, Q., Li, Y., Ding, H., Ma, A., Jiang, J., Chen, G., et al. Microstructure and Mechanical Properties of SiCp/AZ91 Composites Processed by a Combined Processing Method of Equal Channel Angular Pressing and Rolling. *J. Mater. Res. Technol.* 15 (2021), 5244–5251. doi:10.1016/j.jmrt.2021.11.005

Yu, W., Chen, J., Ming, W., An, Q., and Chen, M. Experimental and FEM Study of Cutting Mechanism and Damage Behavior of Ceramic Particles in Orthogonal Cutting SiCp/Al Composites. *Ceram. Int.* 47 (2021), 7183–7194. doi:10.1016/j.ceramint.2020.11.07

Yuan, Z., Shen, Q., Liu, H., Ma, X., Zhang, X., Fu, Q., et al. (2021). Damage Behavior and Mechanism of SiCp/Al Composites under Biaxial Tension. *Mater. Charact.* 180, 111402. doi:10.1016/j.matchar.2021.111402

Zhang, J. F., Zhang, X. X., Wang, Q. Z., Xiao, B. L., and Ma, Z. Y. (2018). Simulation of Anisotropic Load Transfer and Stress Distribution in sicp/Al Composites Subjected to Tensile Loading. *Mech. Mater.* 122, 96–103. doi:10.1016/j.mechmat.2018.04.011

Zhao, G., Zhang, L., Tang, C., Hao, W., and Luo, Y. (2019). Clustering of AE Signals Collected during Torsional Tests of 3D Braiding Composite Shafts Using PCA and FCM. *Compos. Part B Eng.* 161, 547–554. doi:10.1016/j.compositesb.2018.12.145

Zhao, G., Zhang, L., Wang, B., Hao, W., and Luo, Y. (2019). HHT-based AE Characteristics of 3D Braiding Composite Shafts. *Polym. Test.* 79, 106019. doi:10.1016/j.polymertesting.2019.106019

Zhu, C., Gu, P., Wu, Y., Liu, D., and Wang, X. (2019). Surface Roughness Prediction Model of SiCp/Al Composite in Grinding. *Int. J. Mech. Sci.* 155, 98–109. doi:10.1016/j.ijmecsci.2019.02.025

Conflict of Interest: The authors declare that the research was conducted in the absence of any commercial or financial relationships that could be construed as a potential conflict of interest.

Publisher's Note: All claims expressed in this article are solely those of the authors and do not necessarily represent those of their affiliated organizations, or those of the publisher, the editors and the reviewers. Any product that may be evaluated in this article, or claim that may be made by its manufacturer, is not guaranteed or endorsed by the publisher.

Copyright © 2022 Wu, Wei, Wang, Sha and Hao. This is an open-access article distributed under the terms of the Creative Commons Attribution License (CC BY). The use, distribution or reproduction in other forums is permitted, provided the original author(s) and the copyright owner(s) are credited and that the original publication in this journal is cited, in accordance with accepted academic practice. No use, distribution or reproduction is permitted which does not comply with these terms.